

Investigation of the Mn Binding Site in Cytochrome *c* Oxidase from *Paracoccus denitrificans* by High-Frequency EPR

Hanno Käss,[†] Fraser MacMillan,[‡] Bernd Ludwig,[§] and Thomas F. Prisner^{*,‡}

Department of Physical Chemistry III, Darmstadt University of Technology, Petersenstrasse 20, D-64287 Darmstadt, Germany, and Institute of Physical and Theoretical Chemistry and Institute of Biochemistry, Johann Wolfgang Goethe-University Frankfurt, Marie-Curie-Str. 9-11, D-60439 Frankfurt, Germany

Received: September 3, 1999; In Final Form: March 20, 2000

Cytochrome *c* oxidase contains a redox-inactive metal center of unknown function. It has been shown that for *Paracoccus denitrificans*, depending on growth conditions, Mn²⁺ ions can occupy the Mg²⁺ site in the functional protein. Differences between the 9.5 GHz X-band electron paramagnetic resonance (EPR) spectra of such Mn²⁺ preparations in oxidized and reduced state have previously been interpreted as being due to conformational changes. However, only minor differences have been found in analogous 34 GHz Q-band EPR experiments on Mn²⁺ containing cytochrome *c* oxidase from *Rhodobacter sphaeroides*. The new temperature-dependent X-, Q- and 95 GHz W-band EPR data from *Paracoccus* preparations shown here provide a consistent explanation of these contrasting former interpretations. The EPR spectra of oxidized samples reveal contributions of a dipolar interaction between the Mn²⁺ spin and the paramagnetic dinuclear Cu_A center. In reduced samples, the Cu_A center is diamagnetic, and thus, a pure Mn²⁺ signal is found. The zerofield parameters *D* and *E* are 145 ± 10 (120 ± 5) G and 28 ± 5 (22 ± 3) G in the fully oxidized (reduced) protein. From the evaluated dipolar coupling constant of 33.6 ± 1 G, an averaged distance between Mn²⁺ and the Cu_A center of 9.4 ± 0.2 Å was calculated, providing an independent confirmation of the distance calculated from the 2.7 Å X-ray structure.

1 Introduction

Cytochrome *c* oxidase is the terminal enzyme of most biological respiratory chains located in the inner membrane of mitochondria and the cytoplasmic membrane of bacteria.^{1,2} It mediates two closely coupled biochemical processes: (i) electron transfer from cytochrome *c* to molecular oxygen with the formation of water and (ii) proton translocation across the membrane. The latter results in the storage of energy on a molecular scale by building up a transmembrane electrochemical gradient, which is then used in the synthesis of adenosine triphosphate (ATP). Taken together, these results allow cytochrome *c* oxidase to be regarded as a redox-linked proton pump.^{3,4}

The mitochondrial protein complex has a molecular weight of about 200 kDa. It consists of 3 large subunits and up to 10 additional small subunits. The bacterial enzymes typically contain 2–4 different subunits being of considerable sequence homology with the respective three largest mitochondrial subunits. Recently, the crystal structures of cytochrome *c* oxidase prepared from the soil bacterium *P. denitrificans* and from

bovine heart have been analyzed by X-ray diffraction to 2.7 and 2.3 Å resolutions, respectively.^{5–9}

Four redox active metal centers are found in *Paracoccus* and bovine heart cytochrome *c* oxidase: Subunit I contains a low-spin heme molecule (a) and a second high-spin heme (a₃) neighboring a mononuclear Cu center (Cu_B). A second, binuclear Cu center (Cu_A) is located in subunit II. The geometry of the metal centers in cytochrome *c* oxidase and their immediate surroundings according to the 2.7 Å X-ray structure⁸ is shown in Figure 1. The electron-transfer proceeds as follows: Cytochrome *c* → Cu_A → a → center (a₃, Cu_B). An extended family of related enzymes exists in which different heme types replace both the low-spin and high-spin hemes. Nevertheless, this family of heme-copper terminal oxidases shows structural and functional homology in its O₂ reduction site and chemistry.⁴ It must be noted that cytochrome *c* oxidase preparations from *Paracoccus* containing solely the two large subunits I and II are fully competent in electron transfer and energy transduction in vitro.¹⁰

Despite the large body of experimental data collected for cytochrome *c* oxidase (e.g., refs 2–6) some fundamental questions still remain. One of them is the function of an additional and redox-inactive metal binding site located between subunits I and II.^{5,6} For a series of bacterial cytochrome *c* oxidase preparations, it was shown that this site could bind Mn as well as Mg.^{10–12} Interestingly, the ratio of Mg to Mn bound to the protein can be altered by choosing appropriate growth conditions, without affecting the enzymatic activity of the cytochrome *c* oxidase complex.^{10,12} This finding opened the way for a selective investigation of that metal site by monitoring the characteristic EPR signature of Mn²⁺. Already in 1981, EPR experiments revealed slight differences in the Mn²⁺ EPR spectra

* To whom correspondence should be addressed. E-mail: prisner@chemie.uni-frankfurt.de. Fax: 49 69 798 29 404.

[†] Department of Physical Chemistry III, Darmstadt University of Technology.

[‡] Institute of Physical and Theoretical Chemistry, Johann Wolfgang Goethe-Universität Frankfurt.

[§] Institute of Biochemistry, Johann Wolfgang Goethe-Universität Frankfurt.

^{||} Throughout this paper, the amino acid residues will be labeled in analogy to the 2.7 Å X-ray data from *P. denitrificans* (see ref 8), documented in file 1ar1.pdb of the Brookhaven Protein Database.

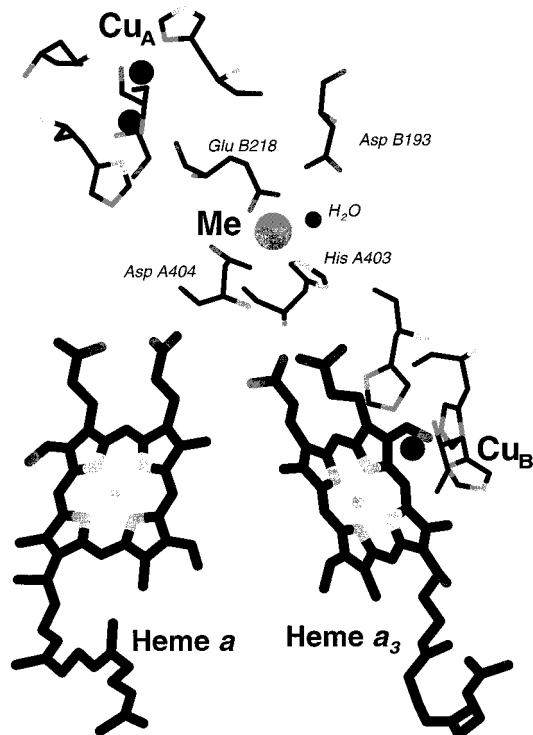


Figure 1. Geometry of the redox-active cofactors participating in the electron-transfer process mediated by cytochrome *c* oxidase. The atom labeled with “Me” indicates the position of the additional metal center of unknown function. Coordinates taken from the 2.7 Å X-ray structure determined for the *Paracoccus denitrificans* protein (see ref 8). Only part of the immediate surroundings of the respective cofactors is shown.

of oxidized and reduced cytochrome *c* oxidase from *P. denitrificans*.¹⁰ Later, these changes were interpreted as being due to conformational modifications of the cytochrome *c* oxidase complex close to the Mn/Mg binding site, accompanying the change of the oxidation state of the Cu_A center.¹¹ In addition to these investigations, detailed cw- and pulsed EPR experiments on cytochrome *c* oxidase preparations from wild-type and genetically engineered *R. sphaeroides* led to the conclusion that the Mn/Mg site might act as a link between subunits I and II, thus having at least some structural function.^{12,13} However, in contradiction to the earlier work^{10,11} no clear change in the X-band cw-EPR spectra between samples with Cu_A either in oxidized or in reduced state was found.

The X-ray data from bovine heart cytochrome *c* oxidase, which revealed that glutamate B218¹¹ was coordinated to Cu_A on one side and Mg on the other side, led to an exciting proposal: Because Cu_A is involved in electron transfer, it was suggested that the oxidation state of the metal in the Mn/Mg binding site might control the transfer process itself.⁷ It must be noted here that site-directed mutagenesis in combination with EPR independently showed that Glu B218 and also Asp B193 are essential in the binding of manganese/magnesium in the cytochrome *c* oxidase complex.¹⁴

This work presents a reinvestigation of the Mn/Mg binding site in cytochrome *c* oxidase, employing the recently established methodology of high-frequency EPR. To disentangle the different EPR signals of the protein complex, cytochrome *c* oxidase isolated from *P. denitrificans* grown on Mn containing medium^{15,16} has been investigated by X-band (9 GHz), Q-band (35 GHz) and, in particular, W-band (95 GHz) EPR. This allows a complete explanation of the Mn²⁺ spectra taken at the different microwave frequencies and results in a satisfying and consistent interpretation of the previously published EPR

data.^{10,11,13} In addition, our data provide detailed information about the local geometry of the Mn/Mg binding site in cytochrome *c* oxidase without the need for X-ray experiments. Thus, the EPR data can be taken as an independent confirmation of important features of the cytochrome *c* oxidase X-ray structure.

2 Materials and Methods

2.1 Preparation. *P. denitrificans* strain ATCC 13 543 was grown on methylamine as carbon source in a standard medium containing 50 μM manganese chloride.¹⁵ The four-subunit cytochrome *c* oxidase was isolated from the membrane fraction after solubilization, using n-dodecyl-β-D-maltoside, as described earlier.¹⁶ In the following, the cytochrome *c* oxidase samples resulting from this preparation without any subsequent chemical treatment are referred to as being *oxidized* because their Cu_A center is in its oxidized state. The addition of 25 mM of dithionite resulted in reduced samples containing *reduced* Cu_A. The EPR spectra presented below were taken on samples with a protein concentration of about 200 μM.

2.2 EPR-Spectroscopy. X-Band (9.5 GHz) EPR spectra were taken using a standard Bruker ESP300 setup equipped with an helium flow Oxford ESR A 900 cryostat and a rectangular TE₁₀₂ microwave cavity Bruker ER 4102 ST. The Q-band (34 GHz) experiments were performed using a Bruker ER 200 D console and a TE₁₁₀ cavity Bruker ER 5106 QT without an ENDOR coil. The temperature was controlled using an Oxford CF 935 helium flow cryostat. The microwave frequency was determined with an HP 5352 counter, and the magnetic field was determined by a Bruker gaussmeter. The W-band (94 GHz) data were measured using a Bruker EleXsys E680 W-band spectrometer, equipped with a helium flow Oxford CF 935 cryostat, a cylindrical Bruker Teraflex TE₁₁₀ cavity, and a 6T Magnex superconducting magnet. The microwave frequency was measured with the internal Bruker counter. Both oxidized and reduced cytochrome *c* oxidase samples were investigated at all three microwave frequencies in a temperature range from 10 to 140 K.

2.3 Simulation of EPR Spectra. The EPR spectra were simulated in the framework of a third-order perturbation theory treatment of the spin Hamiltonian describing the Mn²⁺ ($S = 5/2$, $I = 5/2$) center.¹⁷

$$\hat{H} = g_e \mu_B B_0 \hat{S}_Z - g_i \mu_i B_0 \hat{I}_Z + a \hat{I} \hat{S} + \hat{S} D_{\text{ZFS}} \hat{S} \quad (1)$$

Here, the symbols have their usual meaning, a is the isotropic hyperfine coupling (hfc) constant, g_e and g_i are the isotropic electron and nuclear g-factor, respectively, μ_B is the Bohr magneton, μ_i is the nuclear magneton, B_0 is the static magnetic field, and D_{ZFS} is the zero field splitting (ZFS) tensor. In the case of disordered samples, the EPR signal is dominated by the central $|+1/2, m_1\rangle \leftrightarrow |-1/2, m_1\rangle$ finestructure transitions. The extension of the perturbation treatment for this specific subset of transitions to third-order yields an improved result that describes the slight orientational dependence of the position of the resonant fields of the allowed ($\Delta m_1 = 0$) and forbidden ($\Delta m_1 = \pm 1$) EPR transitions.¹⁷ All of the simulations presented below were calculated using this third-order approximation.

The forbidden transitions show up as five linepairs of less intensity, located between the individual lines of the Mn²⁺ hyperfine sextet. The splitting δ_1 of each of these pairs is independent from the ZFS¹⁸

$$\delta_1 = \frac{17a^2}{2B_0} + \frac{2g_i}{g_e} B_0 \quad (2)$$

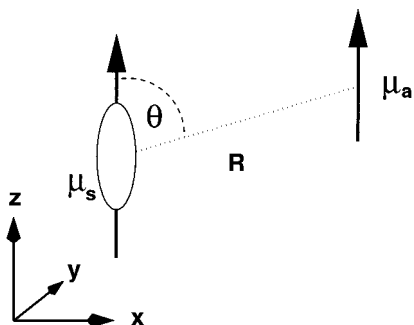


Figure 2. Point dipole model employed in the calculation of ΔB_{dip} . The magnetic moment μ_s of an electron spin located at the position of the Mn^{2+} center interacts with a second magnetic moment μ_a located at the Cu_A position. Vector \mathbf{R} connects both magnetic moments. The orientation of \mathbf{R} with respect to the D_{zz} principal axis of the zero field tensor is given by angle Θ . An ellipsoid has been included in the drawing to symbolize the orientation of the ZFS tensor.

The intensity of the forbidden transitions, relative to that of the allowed ones, is proportional to the ratio $(D/B_0)^2$. Because of that, the spectral features due to forbidden transitions become weaker with increasing magnetic field.

The spectra of reduced cytochrome *c* oxidase could be satisfactorily simulated using the equations given in ref 17. In contrast, in the case of oxidized cytochrome *c* oxidase preparations, an additional term ΔB_{dip} must be included in these third-order expressions to achieve satisfying results. It represents the shift of the resonant lines due to dipolar interaction between the magnetic moment μ_s of the Mn^{2+} electron spin and a second magnetic moment μ_a , located at a distance \mathbf{R} (see Figure 2). In field units, this dipolar coupling can be quantified in the usual way as

$$\Delta B_{\text{dip}} = \frac{1}{\hbar\gamma_e} \frac{\mu_0}{4\pi} \frac{\mu_s \mu_a}{R^3} (3 \cos^2 \theta - 1) = \frac{2}{3} D_{\text{dip}} \cdot (3 \cos^2 \theta - 1) \quad (3)$$

where θ represents the angle between the vectors \mathbf{R} and the D_{zz} principal axis of the zero field tensor axis system, and γ_e is the gyromagnetic ratio of an electron. It must be remembered here that the dipolar interaction is described by a traceless tensor with eigenvalues D_{11} , D_{22} , and D_{33} , where $2D_{11} = 2D_{22} = -D_{33}$. Thus, it can be characterized by the value D_{dip} , where $D_{\text{dip}} = -3/2 D_{33}$.

The positions of the allowed and forbidden transitions were calculated by the analytical formulas given in ref 17. The introduction of the detailed expressions for the transition probabilities, which are also mentioned by Reed and Markham did not improve the quality of the results. Thus, the intensity of all of the allowed transitions was assumed to be equal to one. The contribution of the forbidden transitions was included by introduction of a constant weighting factor between 0 and 1 for their intensity, depending on microwave frequency. A standard powder average with angular steps of 0.9° between neighboring orientations on the unit sphere was calculated, assuming Lorentzian line shapes for the individual transitions. The whole simulation routine was programmed using MATLAB 5.1, a program created by The MathWorks Inc., Natick MA. This program ran under Windows NT 4.0 on a Pentium 133 MHz PC, the typical computing time for a single simulation was about 3 min.

3 Results and Evaluation

3.1 Experiments. In addition to the six-line hyperfine pattern of the Mn center being of particular interest in the present work,

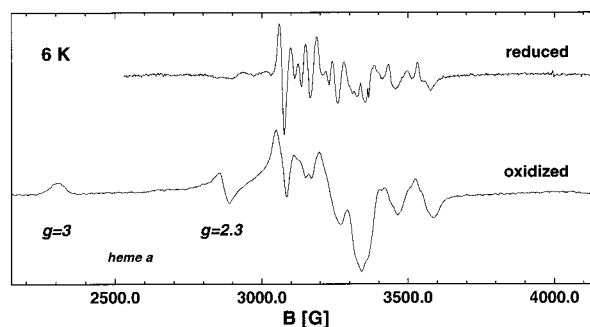


Figure 3. Comparison of low temperature X-band (9.5 GHz) spectra of oxidized and chemically reduced cytochrome *c* oxidase. Experimental conditions: $T = 6$ K; microwave power = 20 mW; field modulation amplitude = 5 G; effect modulation frequency = 100 kHz; time constant = 163 ms; total measuring time = 500 s.

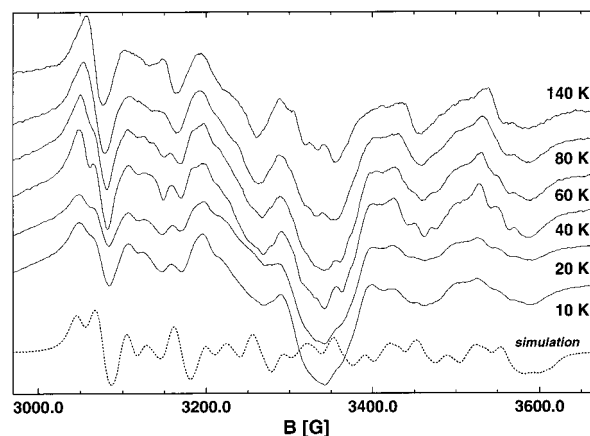


Figure 4. X-band spectra of oxidized cytochrome *c* oxidase, taken at temperatures between 10 and 140 K (solid lines). A simulation calculated using the optimum parameters (see text) is included (dotted line). Experimental conditions: microwave power = 20 mW; field modulation amplitude = 5 G; effect modulation frequency = 100 kHz; time constant = 163 ms; total measuring time = 500 s. Simulation parameters: $D = 145$ G; $E = 28$ G; $a = 96.5$ G; $D_{\text{dip}} = 33.6$ G; $\Theta = 75^\circ$; $\Psi = 0^\circ$; $\Delta B_{1/2} = 22$ G; intensity ratio of forbidden to allowed transitions = 0.5.

the four redox-active metal centers of cytochrome *c* oxidase give rise to a series of other well-known EPR signals. These signals in oxidized cytochrome *c* oxidase are as follows: (i) the oxidized binuclear Cu_A center exhibiting a powder pattern with $g_x = 2.00$, $g_y = 2.03$ and $g_z = 2.18^{10,19,20}$; (ii) the high spin ferric heme a_3 resulting in signals at $g_{\perp} = 6$ and $g_{\parallel} = 2$; 21,22 (iii) the low spin ferric heme a causing patterns at $g = 3.07$, 2.25 , and 1.45 [22]; (iv) the Cu_B center showing structures at $g_{\parallel} = 2.23$ and $g_{\perp} = 2.05$ [22].

X-Band Data. Low-temperature X-band spectra of both oxidized and reduced cytochrome *c* oxidase are compared in Figure 3. The oxidized sample exhibits the expected sextet of rather broad lines around $g = 2.0$, which is superimposed on an extended underlying structure due to the Cu_A center. In addition a series of different signals at g -values of 2.3, 3 and 6 is observed, representing the contributions of the hemes. The reduced sample yields a nicely structured spectrum centered at $g = 2.0$.

Detailed spectra of oxidized and reduced cytochrome *c* oxidase were taken between 10 and 140 K. Figure 4 reveals that the intensity of the broad structure around the $g = 2.0$ region in the oxidized sample reduces with increasing temperature. In addition, some minor features also change, in particular the shape of the leftmost prominent line at 3060 G is varying. Up

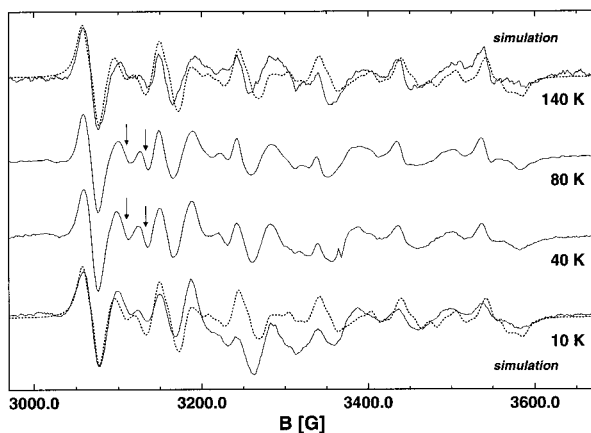


Figure 5. X-band spectra of chemically reduced cytochrome *c* oxidase measured between 10 and 140 K (solid lines). The optimum simulation (see text) is shown together with the 10 and 140 K spectra (dotted lines). Experimental conditions: similar to Figure 4; microwave power = 20 mW; field modulation amplitude = 5 G; effect modulation frequency = 100 kHz; time constant = 163 ms; total measuring time = 500 s. Simulation parameters: $D = 120$ G; $E = 22$ G; $a = 96.5$ G; $\Delta B_{1/2} = 17$ G; intensity ratio of forbidden to allowed transitions = 0.5.

to 40 K, it clearly exhibits either a shoulder or is even split into a doublet by somewhat more than 20 G. At higher temperatures this pattern gradually collapses and at 140 K only a single line remains. As can be seen in Figure 5, however, the spectrum of reduced cytochrome *c* oxidase is essentially unaffected by changes in this temperature range. Its structure, though, is still rather complicated. An interesting feature is observed in the low-field region of the spectra. A closely spaced linepair exhibiting a splitting of about 25 G appears. This is indicated by the arrows on the spectra taken at 40 and 80 K in Figure 5.

It is somewhat questionable to evaluate the line widths from these X-band spectra because many of the individual lines are strongly overlapping. A trend, however, can be seen, when considering the first prominent line at 3060 G on the low-field side of the spectrum in the data sets measured at 140 K. In the case of the oxidized sample, it has a line width $\Delta B_{pp} \approx 20$ G, in reduced cytochrome *c* oxidase, it is about 17 G. The intensity of the spectral components reduces slightly with increasing magnetic field.

Q-Band Data. Temperature-dependent Q-band spectra of both oxidized and reduced cytochrome *c* oxidase are shown in Figures 6 and 7. Because of the g -value differences between the Mn center and the other EPR active centers in cytochrome *c* oxidase, and, in addition, the experimental magnetic field B_0 being clearly above low-field conditions in Q-band, their respective spectral features are better separated from each other as compared to X-band. At temperatures down to 100 K, oxidized cytochrome *c* oxidase exhibits a typical Mn^{2+} hyperfine pattern, the individual lines have a width ΔB_{pp} of about 14 G. However, below 50 K, each of the six hyperfine lines splits into a line pair showing a spacing of somewhat more than 20 G. An intermediate range is found between 50 and 100 K, in which a central line arises within the respective doublets.

The Q-band spectra of reduced cytochrome *c* oxidase, however, consist of the characteristic Mn^{2+} pattern with additional line pairs of low intensity due to the forbidden transitions, split by 15.4 G. The line width of the dominating sextet lines is around 10 G, their averaged spacing is 96.4 G. No temperature dependent changes were detected. For both oxidized and reduced cytochrome *c* oxidase, the intensity of

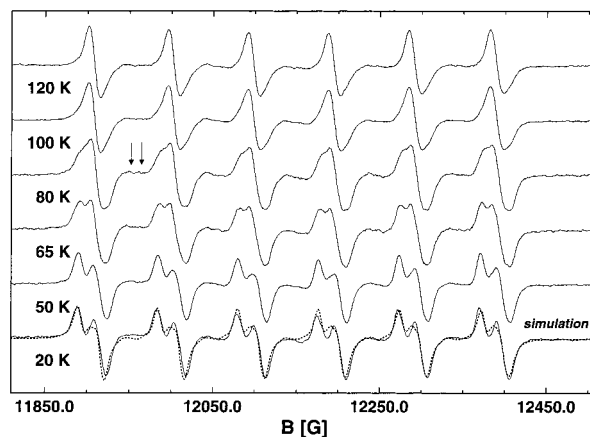


Figure 6. Q-band spectra of oxidized cytochrome *c* oxidase for temperatures from 20 to 120 K (solid lines). The optimum simulation is included (dotted line). Experimental conditions: microwave power between $0.43 \mu\text{W}$ (20 K) and $43 \mu\text{W}$ (120 K); field modulation amplitude = 3.6 G; effect modulation frequency = 12.5 kHz; time constant = 160 ms; total measuring time = 600 s. Simulation parameters: same as in Figure 4, with the exception of $\Delta B_{1/2} = 14$ G; ratio of transition intensities = 0.06.

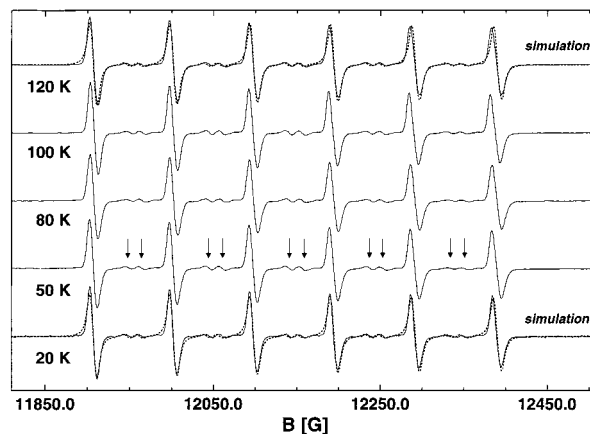


Figure 7. Q-band spectra of reduced cytochrome *c* oxidase measured between 20 and 120 K (solid lines). The optimum simulation is shown together with the 10 and the 120 K spectra. Experimental conditions: identical to Figure 6. Simulation parameters: as in Figure 5, with the exception of $\Delta B_{1/2} = 11$ G; ratio of transition intensities = 0.06.

the individual lines reduces with increasing field, in combination with a slight increase of line width to $\Delta B_{pp} \approx 16$ and 12 G, respectively.

W-Band Data. Figures 8 and 9 show temperature-dependent W-band spectra of oxidized and reduced cytochrome *c* oxidase. Down to 100 K, oxidized cytochrome *c* oxidase exhibits a typical Mn^{2+} hyperfine pattern centered around a g -value of $2.0012 (\pm 0.0001)$, with individual line widths of $\Delta B_{pp} \approx 8$ G and an averaged splitting of $96.45 (\pm 0.05)$ G. The latter value is a clear indication that the manganese atom is coordinated by six ligands.¹⁷ In a manner analogous to the Q-band experiments, below 50 K, these lines split up by more than 20 G. Again, an intermediate range is found between 50 and 100 K, in which the spectrum changes from its low-temperature structure consisting of six doublets to the usual hyperfine pattern of Mn^{2+} .

Reduced cytochrome *c* oxidase shows no temperature-dependent change in its W-band spectrum. At 120 K, the line widths in its typical Mn^{2+} sextet centered around $g = 2.0018 (\pm 0.0001)$ are about 7 G and, again, somewhat narrower as compared to oxidized cytochrome *c* oxidase. The averaged

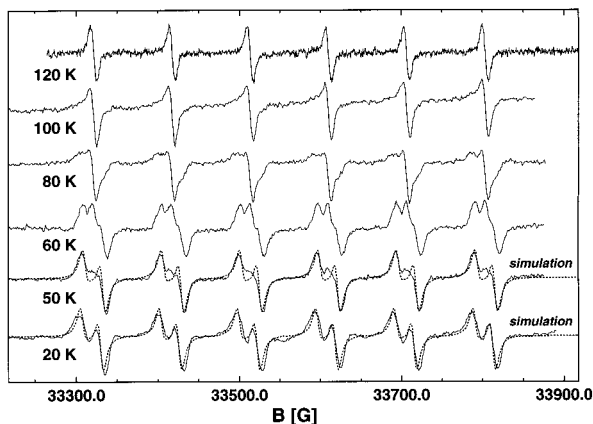


Figure 8. W-band spectra of oxidized cytochrome *c* oxidase taken between 20 and 120 K (solid lines). The optimum simulation is included (dotted line). Experimental conditions: microwave power ≈ 0.6 mW; field modulation amplitude = 3 G; effect modulation frequency = 100 kHz; time constant = 82 ms; total measuring time ≈ 900 s. Simulation parameters: as in Figure 4, with the exception of $\Delta B_{1/2} = 12$ G; ratio of transition intensities = 0.01.

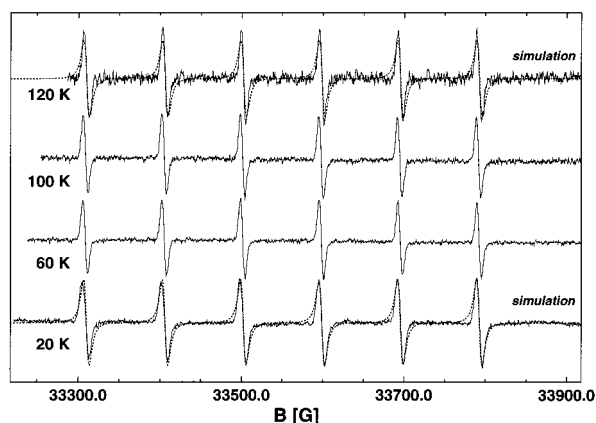


Figure 9. W-band spectra of reduced cytochrome *c* oxidase measured between 20 and 120 K (solid lines). The optimum simulation is included (dotted line). Experimental conditions: microwave power between 0.1 and 0.6 mW; field modulation amplitude 2 G; effect modulation frequency 100 kHz; time constant 82 ms; total measuring time about 900 s. Simulation parameters: as in Figure 5 except $\Delta B_{1/2} = 9$ G; ratio of transition intensities: 0.01.

splitting of the hyperfine lines is $96.40 (\pm 0.05)$ G and, thus, almost the same as that of the oxidized preparations.

Separation of EPR Signals. With the exception of the six line Mn^{2+} pattern, chemically reduced cytochrome *c* oxidase essentially does not show any of the other EPR signals in the $g = 2$ region.^{10,11} A comparison of the X-band spectra in Figure 3 with the Q-band spectra in Figures 6 and 7 and the W-band spectra in Figures 8 and 9 illustrates the fact that W-band EPR is a very convenient way to separate the overlapping heme and Cu signals from the Mn^{2+} hyperfine pattern. Therefore, it is not necessary to employ any subtraction method in order to extract the pure Mn hyperfine signal from Q-band and W-band data sets.

3.2 EPR Spectra of Reduced Cytochrome *c* Oxidase. At first sight, the X-band spectra of reduced cytochrome *c* oxidase presented in Figure 5 look rather complicated. However, comparison with the data taken at other microwave frequencies provides a good understanding of their individual features. In the W-band experiments presented in Figure 9, the samples show the typical Mn^{2+} hyperfine sextet without any additional lines. According to Figure 7, additional linepairs of low intensity show

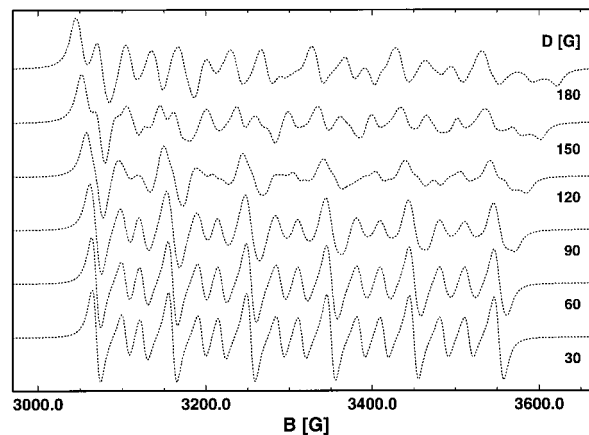


Figure 10. Calculated X-band spectra of reduced cytochrome *c* oxidase, variation of D between 30 and 180 G. Other simulation parameters: $E = 22$ G; $a = 96.5$ G; $\Delta B_{1/2} = 17$ G; ratio of transition intensities: 0.5.

up between the dominating sextet lines at Q-band frequencies. They are indicated by arrows in the spectrum taken at 50 K of Figure 7. These additional lines can also be found in the X-band spectra of Figure 5, on the low field side in particular. Again some of them are indicated by arrows. As compared to the Q-band, their intensity with respect to the hyperfine sextet increases significantly in the X-band. This clearly proves that the lines are due to forbidden $| \Delta m_l | = 1$ EPR transitions of the Mn^{2+} center. Because the ratio $(D/B_0)^2$ decreases with increasing magnetic field, the forbidden transitions do not appear in the W-band EPR spectra. According to eq 2, their splitting depends solely on the hyperfine-coupling constant a present in the Mn^{2+} center. Inserting a value for $a = 96.5$ G, splittings of 15.6 G (26.4 G) in Q-band (X-band) are predicted by theory. This agrees very well with the measured value of 15.4 G (25 G).

3.3 Simulation of Spectra from Reduced Samples. Going from the low-field to the high-field side in the X-band data sets of reduced cytochrome *c* oxidase, the spectral features gradually broaden. Consequently, their resolution clearly decreases. This effect also critically depends on the ZFS parameters D and E .

Figure 10 shows a series of X-band simulations that were computed under variation of D , whereas the parameters E and A were kept fixed at 22 and 96.5 G, respectively. The intensity ratio of the forbidden relative to the allowed transitions was set to a constant value of 0.5, and the homogeneous line width was chosen to be $\Delta B_{1/2} = 17$ G. In particular, the shape of the high-field wing of the spectrum between 3550 and 3650 G exhibits significant changes with increasing D . From this, it is obvious that a value $D > 90$ G is necessary to reproduce the experimental spectra of Figure 5. On the other hand, considering the pronounced modification of the shape of the leftmost line for variation of D , it can similarly be concluded that D must be chosen to be lower than 120 G, in order to model the experimental data.

The simulations in Figure 11 give an idea of how accurately the ZFS parameter E can be determined by comparison of calculations and experiment. Here, a series of simulations for fixed values $D = 120$ G and $A = 96.5$ G is shown, in which only E was varied between 0 and 50 G. Again it is obvious, in particular from the changes of the line shape of the leftmost line, that only a choice of E of about 20 G will model the experiment with satisfying agreement.

The ultimate goal was the determination of a single set of parameters D , E , and A , resulting in a reasonable simulation of both the experimental W-band and the Q-band spectra and in

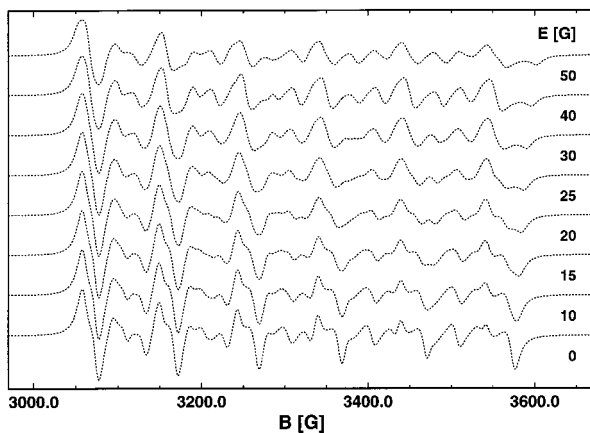


Figure 11. Calculated X-band spectra of reduced cytochrome *c* oxidase, variation of E between 0 and 50 G. Other simulation parameters: $D = 120$ G; $a = 96.5$ G; $\Delta B_{1/2} = 17$ G; ratio of transition intensities = 0.5.

TABLE 1. Zero Field Splitting (ZFS) Parameters D and E , Isotropic Hyperfine Coupling Constant a , Dipolar Interaction D_{dip} , and Relative Orientation Θ of the Principal Axis of the Dipole Coupling Tensor with Respect to the D_{zz} Principal Axis of the ZFS Tensor (see also Figure 2) of the Mn^{2+} Center in Oxidized and Reduced Cytochrome *c* Oxidase, as Evaluated from the Simulations

	D [G]	E [G]	a [G]	D_{dip} [G]	Θ
oxidized	145 (± 10)	28 (± 5)	96.5 (± 0.5)	33.6 (± 1.0)	75° (± 5)
reduced	120 (± 5)	22 (± 3)	96.5 (± 0.5)		

an (at least qualitatively) satisfying agreement with the X-band data of reduced cytochrome *c* oxidase preparations. Because the effect of ZFS on the position of the EPR transitions is proportional to D^2/B_0 , it is evident that D (and E) should be determined in particular with regard to the X-band data, whereas it is a good idea to evaluate a mainly from Q- and W-band data. Concerning the X-band simulations, it should be kept in mind that the perturbation treatment intrinsically leads to poor results if the ratio $D/(g_e \mu_B B_0)$ is not close to zero, i.e., for low microwave frequencies. Reed and Markham mention an upper limit of about 0.05 for that ratio; this may serve as a rule of thumb in order to decide whether the perturbation calculation might yield a useful approximation.¹⁷ Furthermore, it cannot be excluded that a certain spread of D and E values exists in the cytochrome *c* oxidase sample. Thus, the assumption of only two well-defined ZFS parameters, which has been made in the present calculations, is clearly an idealization. Of course, the same is true for the use of an isotropic g -value and an isotropic hyperfine-coupling constant a , which are both justified only by the accuracy of the final result. All of these effects are expected to have minor impact on the resulting simulations. Therefore, they were taken into consideration in a rather qualitative way by simply choosing an appropriate line width for calculation. Resuming, and additionally taking into account that no calculation of transition probabilities has been included in the simulations, the agreement between X-band simulations and experimental spectra is surprisingly good. This leads to the conclusion that the evaluated D and E values are quite reliable, particularly because one did not have to calculate them from the intensity ratios of allowed and forbidden EPR transitions,¹⁸ which are certainly hard to estimate with high accuracy from the experimental data.

Finally, the parameter set given in Table 1 was determined from the simulations. The respective intensity ratio between forbidden and allowed transitions in X-, Q-, and W-band was

set to 0.5, 0.06, and 0.01, respectively. The homogeneous line widths $\Delta B_{1/2}$ used in the calculations for these different microwave frequencies were assumed to be 17, 11, and 9 G, respectively. The simulations calculated with these parameters are included (dotted lines) in Figures 5, 7, and 9. A comparison of experiment and calculation shows that the simulations model the low-temperature data taken at 10 K and the respective 120 K experiments with similar quality. In all of the frequency bands, the experimental spectra are reproduced quite well.

3.4 Splitting of EPR Lines in Oxidized Cytochrome *c* Oxidase. The most striking feature found in the experiments is the doublet splitting of the individual Mn^{2+} hyperfine lines at low temperatures. One could think of several explanations. A simple g tensor effect can certainly be excluded because the splitting is independent of magnetic field.

Another possibility would be the presence of an additional hyperfine interaction in the oxidized system. Because a doublet is revealed in the spectra, this would have to be interpreted as an $I = 1/2$ nucleus coupled by a rather large interaction of more than 20 G to the Mn^{2+} center. Considering the ligand sphere of the Mn^{2+} according to the X-ray structure (cf. Figure 1), the only $I = 1/2$ magnetic moments in close neighborhood are ^1H nuclei of the H_2O ligands; only one out of the three expected ligands was detected by X-ray structure analysis⁸ and ^1H nuclei located in the adjacent His A403, Asp A404, Asp B193, and Glu B218 amino acid residues. A detailed frozen solution ENDOR investigation of Mn^{2+} ligated by water revealed an anisotropic proton hyperfine interaction with a maximum A_{\parallel} tensor eigenvalue of 7.6 MHz ($\cong 2.7$ G).²³ Thus, it can be safely excluded that the doublet splitting arises from such a hyperfine interaction.

However, considering the fact that the splitting is detected only for oxidized samples, and not in the case of reduced cytochrome *c* oxidase, another appealing interpretation of the experimental data exists: In oxidized cytochrome *c* oxidase, the oxidized Cu_A center carries an electron spin ($S = 1/2$), whereas in reduced samples, it is in a diamagnetic ($S = 0$) state. This should result in a magnetic dipole interaction between the Cu_A and the Mn^{2+} center, if the protein is in its oxidized state. The magnitude of this interaction can be estimated by employing eq 3 (see also Figure 2), assuming that both centers carry an electron spin $S = 1/2$. This is reasonable because only the $|+1/2, m_1\rangle \leftrightarrow |-1/2, m_1\rangle$ transitions of the Mn^{2+} center are of interest here. This results in a D_{11} eigenvalue of the dipolar interaction tensor of about $-9285 \text{ G}/R^3$ [\AA] in field units where the distance R between the centers must be inserted in \AA units. According to the X-ray structure,⁸ the distance between Cu_A and Mn^{2+} is about 9.6 \AA , yielding an estimated value of $D_{33} = -2D_{11} = 21$ G ($\cong D_{\text{dip}} = 31.5$ G). Compared to the experimentally detected splitting of somewhat more than 20 G, this qualitative estimate looks quite reasonable. In the following this model is proven quantitatively.

3.5 Simulation of Spectra from Oxidized Samples. To quantify the magnetic dipolar interaction between the Cu_A and the Mn^{2+} center in oxidized cytochrome *c* oxidase, the experimental EPR spectra were simulated on the basis of the theoretical description by Reed and Markham, employing the formulas given in ref 17. The parameters varied in the simulations were again the ZFS parameters D and E , the isotropic hyperfine coupling constant a of electron spin and nuclear spin in the Mn^{2+} center, and the dipolar coupling D_{dip} , together with the Euler angles ψ and θ (because of the symmetry of the problem, the result does not depend on the magnitude of Φ) for the transformation of the eigensystem of the dipolar

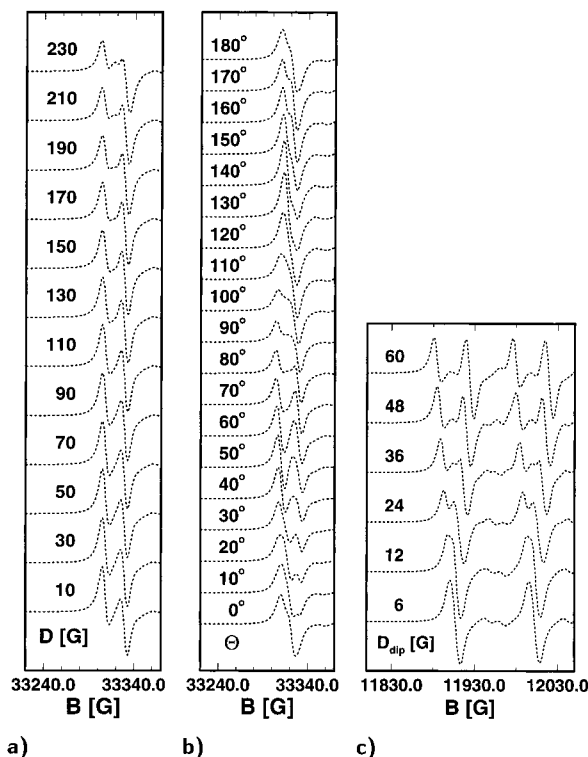


Figure 12. Calculated Q- and W-band spectra of oxidized cytochrome *c* oxidase. (a) W-band simulations for variation of D between 10 and 230 G. Fixed parameters: $E = 28$ G; $a = 96.5$ G; $D_{dip} = 34$ G; $\Theta = 75^\circ$; $\Psi = 0^\circ$; $\Delta B_{1/2} = 12$ G; ratio of transition intensities = 0.01. (b) W-band simulations for variation of angle Θ between 0° and 180° (cf. Figure 2). $D = 145$ G, and all of the other parameters, with the exception of Θ , as before. (c) Q-band simulations for variation of dipolar coupling D_{dip} between 6 and 60 G. Fixed parameters: $D = 145$ G; $E = 28$ G; $a = 96.5$ G; $\Theta = 75^\circ$; $\Psi = 0^\circ$; $\Delta B_{1/2} = 14$ G; ratio of transition intensities = 0.06.

coupling tensor to the ZFS tensor system. In addition, the homogeneous line width of the individual transitions was varied to account for line broadening effects.

Figure 12 gives an idea of the quality of the final result. Figure 12a shows a series of W-band simulations where the ZFS parameter D was varied, whereas all of the other values were fixed. It should be noted that only the leftmost line of the Mn^{2+} hyperfine sextet is shown in this Figure 12a because all of the individual lines of the sextet essentially exhibit the same line shape. The increase of D causes increasing asymmetry of the line shape, in particular, for $D > 90$ G, the absolute peak intensity of the low-field part of the pattern is clearly lower than that of the high-field part. Obviously, D must be set to about 150 G to reproduce the line shape found in the W-band experiments.

Figure 12b illustrates the pronounced dependency of the line shape on the relative orientation of the eigensystems of the dipolar interaction tensor \mathbf{D}_{dip} and the ZFS tensor. In the course of these W-band simulations, the Euler angle Θ between their respective z -axes is varied, whereas all other parameters are kept constant. The line shape depends critically on Θ , for $\Theta \approx 0^\circ$ and 120° , essentially a single line emerges, whereas for Θ around 80° , the simulation yields a clearly split asymmetric doublet, which is very similar to that observed in the Q- and W-band experiments.

Figure 12c shows Q-band simulations for different values of the dipolar coupling constant D_{dip} , whereas the other parameters are constant. The Euler angle Θ was set at 75° , a value resulting in a pronounced doublet splitting. Obviously, a value of about

30 G for D_{dip} results in a satisfying simulation of the experimental data.

For the analysis of oxidized samples, a larger number of parameters, namely D , E , a , D_{dip} , and Θ needed to be determined, as compared with the reduced cytochrome *c* oxidase. Finally, the parameter set given in Table 1 resulted in a reasonable simulation of both the experimental W-band and Q-band spectra and in an, at least qualitatively, satisfying agreement with the X-band data. The respective intensity ratio between forbidden and allowed transitions in X-, Q-, and W-band was set to 0.5, 0.06, and 0.02. The homogeneous line widths $\Delta B_{1/2}$ used in the calculations for these different microwave frequencies were assumed to be 22, 14, and 12 G, respectively.

The simulations calculated with these parameters were included as dotted line spectra in Figures 4, 6, and 8. They reproduce the low-temperature Q- and W-band spectra of oxidized cytochrome *c* oxidase quite well. As mentioned above, it should be remembered that the third-order perturbation theory model used in the calculations will yield poor results for the case of low microwave frequencies. Nevertheless, characteristic features of the experimental X-band spectra, in particular, the splitting of the leftmost line at low temperature and the shape of the right wing on the high field side, are modeled with satisfying agreement. Of course, the central part of the experimental data sets is dominated by the overlapping intense Cu_A signal that will not be reproduced by the simulation.

3.6 Temperature Effects in the EPR Spectra of Oxidized Samples. An intermediate range of temperatures extending from 20 to 100 K exists in which the spectrum of oxidized cytochrome *c* oxidase samples changes in a characteristic way. As can be seen in Figures 4, 6, and 8, the effect is revealed in a similar way in the experimental X- and Q- as well as in the W-band spectra presented in this work. Above 100 K, the system seems to be subject to fairly large relaxation or exchange rates, as compared to the doublet splitting Δ of about 20 G. This gradual collapse of the low-temperature dipolar split line into one single line with increasing temperature has a spectral signature very similar to motional or exchange averaging of interactions as described by the Anderson theory for exchange narrowing. In this case, the temperature-dependent averaging of the dipolar splitting of the Mn hyperfine lines could be introduced by fast spin relaxation of either the Mn or the Cu_A spin system. For example, saturation recovery and cw-saturation EPR experiments on the Cu_A signal in cytochrome *c* oxidase show a strong temperature dependence of the relaxation exactly in this temperature range.^{24,25} This effect could be further enhanced by flip-flop transitions between the coupled spin systems. According to the Anderson model,

$$\Delta B_{1/2} = \left(\frac{\gamma_e}{2\pi}\right) \Delta^2_{dip} T_1 \quad (4)$$

a relaxation time on the order of 10 ns for one of the two spins would be necessary to explain the observed narrowing. Pulsed EPR investigations are in progress to elucidate the source of the temperature dependence of the dipolar averaging in more detail.

4 Discussion

4.1 Interpretation of the Dipolar Coupling Parameters.

It has been shown that the low-temperature EPR spectra of oxidized cytochrome *c* oxidase presented in this work can be explained consistently by the assumption of a magnetic dipolar interaction between a magnetic moment at the Mn^{2+} position

and the magnetic moment of the oxidized Cu_A site ($S = 1/2$). Furthermore, it has been assumed that the effects of a spin exchange coupling J can be neglected. In the framework of this simple point-dipole model, the distance between the interacting spins can be evaluated from the determined dipolar coupling D_{dip} to be $9.4 (\pm 0.2) \text{ \AA}$. According to the 2.7 \AA X-ray structure model of the *Paracoccus* cytochrome *c* oxidase complex,⁸ the distance between the Mn atom and the geometrical center of the Cu_A site is 9.6 \AA . These two independently determined values agree very well. This demonstrates the high precision that can be achieved when EPR is employed as a means of measuring distances in the range of about 10 \AA . In addition, this agreement demonstrates that J must indeed be very small.

However, due to their accuracy, the EPR results are not simply a confirmation of the X-ray data set. According to the X-ray structure, the distances between the Mn atom and the individual Cu atoms in the binuclear Cu_A site are 9.0 and 10.3 \AA , respectively. The evaluated distance of $9.4 (\pm 0.2) \text{ \AA}$ between the electron spins of the Mn^{2+} center and the oxidized Cu_A center indicates that the electron spin is shared between both Cu atoms. This agrees nicely with the previous interpretation of this center as a mixed valence $[\text{Cu} (1.5) \dots \text{Cu} (1.5)]$ dinuclear complex carrying an electron spin $S = 1/2$ distributed over the copper atoms and the bridging ligands. This proposal was first made by Kroneck²⁶ and has since been supported by numerous EPR,^{20,27} ENDOR,^{28,29} ESEEM,³⁰ and NMR^{31,32} experiments as well as theoretical investigations^{27,33} of the binuclear Cu_A center in cytochrome *c* oxidase and its closely related counterpart in nitrous-oxide reductase.

EPR provides further insights concerning the atoms ligating the Mn site. Four of them could be resolved directly by X-ray structure analysis. These are the N_ϵ atom of His A403, two oxygen atoms of Glu B218 and Asp A404, and the oxygen atom of a H_2O molecule acting as a kind of bridge between the Mn atom and the nearby Asp B193 residue. As can be seen in Figure 13, these four ligands lie in a common plane and are all located at a distance of about 2.15 \AA to the Mn site. According to the X-ray data, the normal to that plane and the line connecting the Mn and the Cu_A site form an angle of 75.4° . Despite the fact that only four ligands show up in the X-ray data set, it has been mentioned previously that the Mn center in cytochrome *c* oxidase is hexacoordinate because the hyperfine coupling constant a , determined to be 96.5 G , is indicative of hexa coordination and not tetra coordination.^{11,13,17}

In extension of these earlier EPR results, the data presented in this work indicate the position of the two remaining ligands, which could not be localized by X-ray measurements. The simulation parameter Θ represents the angle between the orientation of the principal axis of the magnetic dipolar coupling tensor and the magnetic z -axis of the Mn^{2+} system. This magnetic z -axis is parallel to the D_{zz} principal axis of the eigensystem of the ZFS tensor of the Mn^{2+} system. On the other hand, the line connecting the Cu_A and the Mn site is oriented parallel to the principal axis of the magnetic dipolar coupling tensor mentioned above. Thus, taken together, the angle between the D_{zz} principal axis of the ZFS tensor of the Mn^{2+} center in oxidized cytochrome *c* oxidase and the line connecting Cu_A and Mn in the protein complex is $\Theta = 75^\circ (\pm 5^\circ)$.

This value agrees very well with the value of 75.4° for the angle between that connecting line and the normal to the plane defined by the four ligands, which have been resolved by X-ray structure analysis. Considering the fairly good axiality of the ZFS tensor (its ratio E/D is rather low) together with the geometry of the ligands according to the X-ray results, this leads

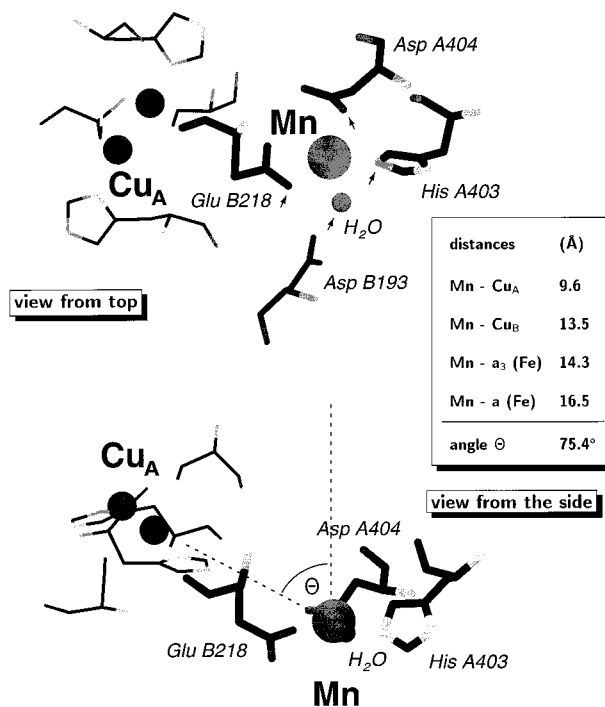


Figure 13. X-ray structure of the immediate surroundings of the Mn center in *Paracoccus* cytochrome *c* oxidase (see ref 8). Upper part: View from top. According to the X-ray data, the Mn atom is axially ligated by four ligands lying together in a common plane. These ligands, marked by arrows, are the amino acid residues Glu B218, His A403, Asp A404, and a H_2O molecule bridging the space between Mn and Asp B193. Lower part: View from the side. The normal to the plane defined by the four axial ligands of the Mn atom and the line connecting it with the geometrical center of the binuclear Cu_A site include an angle Θ of 75.4° . The length of this connecting line is 9.6 \AA . In addition, the calculated distances to the other redox-active centers are given.

to the conclusion that the principal z -axis of the ZFS tensor will be oriented parallel to the normal of the ligand plane. This, in turn, yields the desired information concerning the position of the two axial ligands missing in the X-ray structure. They will be located on, or close to, the plane normal because, otherwise, the z -axis of the ZFS tensor would not be parallel to it.

4.2 ZFS Parameters and Redox State. As can be seen from the experimental data given by Reed and Markham,¹⁷ the ZFS parameters of $D = 145 (\pm 10) \text{ G}$ and $E = 28 (\pm 5) \text{ G}$ evaluated for the Mn^{2+} center in the oxidized and of $D = 120 (\pm 5) \text{ G}$ and $E = 22 (\pm 3) \text{ G}$ in the reduced cytochrome *c* oxidase protein from *P. denitrificans* are rather low for biological systems. Similar results have already been found by Espe (1995) for cytochrome *c* oxidase from *R. sphaeroides*, in which the respective values evaluated from Q-band spectra were $D = 115 (\pm 25) \text{ G}$ and $E = 25 (\pm 15) \text{ G}$ in oxidized and $D = 125 (\pm 20) \text{ G}$ and $E = 45 (\pm 5) \text{ G}$ in reduced cytochrome *c* oxidase.¹³ (However, a slight discrepancy should be noted. From their respective X-band data, Espe et al. excluded the occurrence of E values larger than 25 G in the reduced protein.)

The present work has shown, however, that, apart from ZFS, hyperfine coupling, and general line broadening processes, two additional effects must be taken into account when modeling EPR spectra of the Mn^{2+} center in oxidized cytochrome *c* oxidase: (i) the magnetic dipole interaction between Mn^{2+} and the Cu_A site; (ii) a spin relaxation process exhibiting rates much larger than 10 MHz for temperatures rising above 100 K . As it has been pointed out in detail, both effects severely affect the

experimentally detected line shapes. Because they have not been observed and included in previously published investigations, one should be cautious when comparing D and E parameters given in this work with data published earlier.

In general, the ZFS parameters evaluated for the *Paracoccus* system are similar to those of the *Rhodobacter* protein.¹³ In case of reduced cytochrome c oxidase — where the additional effects mentioned above will not be present — the D parameters are identical within the accuracy of the evaluation. Concerning E , the value of 22 G evaluated for the *Paracoccus* protein may be taken as a clear confirmation of the assumption made by Espe (1995) that E decreases upon enzyme reduction and that it would certainly be less than 25 G, despite the discrepancies between the X- and Q-band evaluations discussed by these authors.¹³ In the case of oxidized *Rhodobacter* cytochrome c oxidase, an approximate value of $D = 150$ G was calculated from the ratio of line intensities in an X-band spectrum taken at 110 K.¹³ It must be noted that the detailed comparison of experimental and calculated spectral features in three different frequency bands, as outlined in the present work, will certainly yield more confident results than a simple estimation from line intensities. A severe drawback of the latter is the fact that the individual line intensities in the experimental Mn^{2+} spectra are rather hard to quantify because of partial overlap. In addition, the present work reveals that the spectral patterns at 110 K are dominated mainly by a spin-exchange narrowing process. This is a fundamental problem for all of the evaluations referring to EPR data on cytochrome c oxidase measured at temperatures well above that of liquid helium. Nevertheless, the number given for *Rhodobacter*¹³ fits quite well to the value of $D = 145$ G in the case of the *Paracoccus* protein. However, the evaluation of ZFS parameters from Q-band data measured on the Mn^{2+} center in oxidized *Rhodobacter* cytochrome c oxidase,¹³ which should be more reliable because it simulates a 150 K spectrum, led to a different result. This raises the interesting question whether differences in the ligand structure of the Mn^{2+} center exist between both protein complexes. Unfortunately, it cannot be answered as long as there are no low-temperature Q- and W-band data available for cytochrome c oxidase prepared from *R. sphaeroides*.

Another interesting finding is the clear change in D of the Mn^{2+} center from 145 G in oxidized to 120 G in reduced *Paracoccus* cytochrome c oxidase. This might be indicative of a slight modification of the ligand structure of the Mn atom, which could accompany the change of the protein redox-state. According to the conclusions of the related detailed discussion for the *Rhodobacter* system, these structural changes will be lower than 0.2 Å in bond length and 10° in bond angle.¹³ Of course, the same arguments and estimates are valid for the present results on *Paracoccus* cytochrome c oxidase.

It is somewhat unsatisfactory that it has not been possible, until now, to quantify these changes in a better way. However, if there would be a clear difference in the D parameter of the Mn^{2+} center between *Paracoccus* and *Rhodobacter* cytochrome c oxidase, this problem could be resolved. Then, the comparison of high resolution, ENDOR or ESEEM,^{13,34} spectra taken on the oxidized cytochrome c oxidase proteins from both organisms might help to unravel the expected small modifications of the ligand sphere by detection of changes in the measured hyperfine couplings because the underlying signals from Cu_A should be similar in both experiments.

Finally, we want to emphasize once again that the crucial point for the consistent evaluation of D , E , a , D_{dip} and Θ

presented here was the availability of experimental X-, Q-, and, in particular, W-band data. The main reason for our confidence in the final results given in Table 1 is that the same respective parameter sets yield satisfying simulations for all of the investigated frequency bands. The remaining imperfections of the simulations must be due to the simplifications, which have already been discussed above. However, it is obvious that they are clearly justified by the quality of the results achieved.

4.3 Consistent Interpretation of Previously Published Data. The pioneering X-band EPR experiments on the Mn^{2+} center in cytochrome c oxidase from *P. denitrificans* showed some qualitative differences between oxidized and reduced samples, in particular changes of individual line widths. Thus, it was suggested that a structural modification of the protein might accompany the change of its redox state.¹⁰ However, because these experiments were performed at temperatures above 130 K, they could not reveal the complete spectral information presented here. Later, a detailed low-temperature EPR investigation was performed. The respective X-band spectra taken at 12 K are essentially identical to those shown in Figures 4 and 5. Again, the data were interpreted in the framework of a conformational change. It was assumed that these structural modifications of the protein would depend on the redox state and lead to two different coordination environments of Mn^{2+} . No attempt was made to evaluate D and E quantitatively.¹¹ The possibility of a magnetic coupling between Mn^{2+} and the Cu_A site was mentioned in that contribution. However, from measured saturation profiles of the Mn^{2+} signal, it was concluded that no such spin–spin interaction would be present in the cytochrome c oxidase protein.

A thorough investigation of the Mn^{2+} binding site in cytochrome c oxidase from *R. sphaeroides* followed, employing X- and Q-band EPR as well as site-directed mutagenesis to alter the ligand sphere of that metal center.^{12,13} Because the Q-band experiments were performed at 150 K, the significant low-temperature spectral changes were not detected. The magnitude of the Mn^{2+} ZFS parameters was evaluated. However, the resulting changes of D and E between oxidized and reduced cytochrome c oxidase were rather small ($\Delta D = 10$ G; $\Delta E \leq 25$ G). From this, it was concluded that only minor changes in the structure of the Mn^{2+} binding site would occur.

The results presented in this work resolve the discrepancy between the contradictory conclusions made in the earlier investigations. The differing spectral features in the low-temperature X-band spectra of oxidized and reduced cytochrome c oxidase are due to magnetic spin–spin interaction between the Mn^{2+} center and the Cu_A site. Thus, their interpretation in terms of a structural change of the Mn^{2+} binding site^{10,11} can certainly be excluded. However, a distinct reduction of the ZFS parameters, in particular of D , was found to accompany the change from the oxidized to the reduced state in cytochrome c oxidase from *P. denitrificans*. This might be indicative of a minor, but significant, modification of the coordination sphere of Mn^{2+} in that protein complex, which could be interpreted, at least to some extent, to favor the former hypothesis of conformational changes.^{10,11}

The difference in the Mn^{2+} ZFS parameters between oxidized cytochrome c oxidase from *R. sphaeroides*¹³ and *P. denitrificans* may prove to be an interesting result. This problem certainly requires further experimental investigation. If confirmed, these results may open the way to further insight into the structure and function of the ligand sphere surrounding the nonredox-active metal center.

5 Conclusion

This work demonstrates that high-field EPR, in particular in the framework of a multi-frequency EPR approach, can provide detailed structural information about the immediate surroundings of the nonredox-active metal center in cytochrome *c* oxidase. Considering the requirements on the investigated preparations, it must be noted that all of the results presented were evaluated from experiments on frozen solution samples. There was no need to investigate protein crystals in order to obtain the desired structural information.

It has also been shown that there is no evidence for major structural modifications of the cytochrome *c* oxidase protein complex accompanying the change of its redox state, as had been suggested earlier.^{6,10,11} Instead, the splitting of the Mn²⁺ hyperfine lines could be qualitatively described by a purely dipolar spin–spin interaction between the paramagnetic Mn²⁺ ion and the binuclear Cu_A center, the evaluated distance being in full agreement with the X-ray structure. This excludes a strong exchange coupling between the Mn and the Cu_A center, thereby confirming the assumption that the Mn site does not participate in the electron-transfer process. Nevertheless, distinct changes of the ZFS parameters have been detected. They are indicative of a minor change in the ligand sphere of the metal center itself. Interestingly, in the case of cytochrome *c* oxidase protein from *R. sphaeroides*, the respective changes of ZFS parameters were found to be smaller.¹³ The reason for that is not known and requires further investigation.

In extension to the results shown here, the Mn atom substituted to this metal binding site has proven to be a powerful probe to determine distances to and spin moments of the other redox-active cofactors in the cytochrome *c* oxidase protein complex. Related EPR investigations are in progress in our laboratory.

Acknowledgment. We gratefully acknowledge the generous permission of Prof. Dr. Wolfgang Lubitz to use the Q-band EPR spectrometer in his laboratory in the Max-Volmer-Institut für Biophysikalische Chemie und Biochemie at the Technical University of Berlin (Germany). The W-band experiments were performed in the laboratory of Prof. Dr. Klaus-Peter Dinse at the Darmstadt University of Technology in the framework of the Schwerpunktprogramm Hochfeld-ESR, which is organized by the Deutsche Forschungsgemeinschaft. The work was supported by the Sonderforschungsbereich 472 of the Deutsche Forschungsgemeinschaft.

References and Notes

- (1) Trumpower, B. L.; Gennis, R. B. *Annu. Rev. Biochem.* **1994**, *63*, 675.
- (2) Michel, H.; Behr, X.; Harrenga, A.; Kannt, A. *Annu. Rev. Biophys. Biomol. Struct.* **1998**, *27*, 329.

- (3) Malmström, B. G. *Chem. Rev.* **1990**, *90*, 1247.
- (4) Babcock, G. T.; Wikström, M. *Nature* **1992**, *356*, 301.
- (5) Iwata, S.; Ostermeier, C.; Ludwig, B.; Michel, H. *Nature* **1995**, *376*, 660.
- (6) Tsukihara, T.; Aoyama, H.; Yamashita, E.; Tomizaki, T.; Yamaguchi, H.; Shinzawa-Itoh, K.; Nakashima, R.; Yaono, R.; Yoshikawa, S. *Science* **1995**, *269*, 1069.
- (7) Tsukihara, T.; Aoyama, H.; Yamashita, E.; Tomizaki, T.; Yamaguchi, H.; Shinzawa-Itoh, K.; Nakashima, R.; Yaono, R.; Yoshikawa, S. *Science* **1996**, *272*, 1136.
- (8) Ostermeier, C.; Harrenga, A.; Ermler, U.; Michel, H. *Proc. Natl. Acad. Sci. U.S.A.* **1997**, *94*, 10 547.
- (9) Yoshikawa, S.; Shinzawa-Itoh, K.; Nakashima, R.; Yaono, R.; Yamashita, E.; Inoue, N.; Yao, M.; Fei, M. J.; Libeu, C. P.; Mizushima, T.; Yamaguchi, H.; Tomizaki, T.; Tsukihara, T. *Science* **1998**, *280*, 1723.
- (10) Seelig, A.; Ludwig, B.; Seelig, J.; Schatz, G. *Biochim. Biophys. Acta* **1981**, *636*, 162.
- (11) Haltia, T. *Biochim. Biophys. Acta* **1992**, *1098*, 343.
- (12) Hosler, J. P.; Espe, M. P.; Zhen, Y.; Babcock, G. T.; Ferguson-Miller, S. *Biochemistry* **1995**, *34*, 7586.
- (13) Espe, M. P.; Hosler, J. P.; Ferguson-Miller, S.; Babcock, G. T.; McCracken, J. *Biochemistry* **1995**, *34*, 7593.
- (14) Witt, H.; Wittershagen, A.; Bill, E.; Kolbesen, B. O.; Ludwig, B. *FEBS Lett.* **1997**, *409*, 128.
- (15) Ludwig, B. *Methods Enzymol.* **1986**, *126*, 153.
- (16) Hendler, R. W.; Pardhasaradhi, K.; Reynafarje, B.; Ludwig, B. *Biophys. J.* **1991**, *60*, 415.
- (17) Reed, G. H.; Markham, G. D. *Biol. Magn. Reson.* **1984**, *6*, 73.
- (18) Weltner, W. *Magnetic Atoms and Molecules*; Dover Publications: Mineola, N. Y., 1989.
- (19) Beinert, H. *Eur. J. Biochem.* **1997**, *245*, 521.
- (20) Antholine, W. E.; Kastrau, D. H. W.; Steffens, G. C. M.; Buse, G.; Zumft, W. G.; Kroneck, P. M. H. *Eur. J. Biochem.* **1992**, *209*, 875.
- (21) Powers, L.; Lauraeus, M.; Reddy, K. S.; Chance, B.; Wikström, M. *Biochim. Biophys. Acta* **1994**, *1183*, 504.
- (22) Fann, Y. C.; Ahmed, I.; Blackburn, N. J.; Boswell, J. S.; Verkhovskaya, M. L.; Hoffman, B. C.; Wikström, M. *Biochemistry* **1995**, *34*, 10 245.
- (23) Tan, X.; Bernardo, M.; Thomann, H.; Scholes, C. P. *J. Chem. Phys.* **1993**, *98*, 5147.
- (24) Scholes, C. P.; Janakiraman, R.; Taylor, H. *Biophys. J.* **1984**, *45*, 1027.
- (25) Brudvig, G. W.; Blair, D. F.; Chan, S. I. *J. Biol. Chem.* **1984**, *259*, 11 001.
- (26) Kroneck, P. M. H.; Antholine, W. E.; Riestler, J.; Zumft, W. G. *FEBS Lett.* **1988**, *242*, 70.
- (27) Neese, F.; Zumft, W. G.; Antholine, W. E.; Kroneck, P. M. H. *J. Am. Chem. Soc.* **1996**, *118*, 8692.
- (28) Gurbel, R. J.; Fann, Y.-C.; Surerus, K. K.; Werst, M. M.; Musser, S. M.; Doan, P. E.; Chan, S. I.; Fee, J. A.; Hoffman, B. M. *J. Am. Chem. Soc.* **1993**, *115*, 10 888.
- (29) Martin, C. T.; Scholes, C. P.; Chan, S. I. *J. Biol. Chem.* **1988**, *263*, 8420.
- (30) Jin, H.; Thomann, H.; Coyle, C. L.; Zumft, W. G. *J. Am. Chem. Soc.* **1989**, *111*, 4262.
- (31) Luchinat, C.; Soriano, A.; Djinovic-Carugo, K.; Saraste, M.; Malmström, B. G.; Bertini, I. *J. Am. Chem. Soc.* **1997**, *119*, 11 023.
- (32) Salgado, J.; Warmerdam, G.; Bubacco, L.; Canters, G. W. *Biochemistry* **1998**, *37*, 7378.
- (33) Karpefors, M.; Slutter, C. E.; Fee, J. A.; Aasa, R.; Källebring, B.; Larsson, S.; Vänngård, T. *Biophys. J.* **1996**, *71*, 2823.
- (34) Hansen, A. P.; Britt, R. D.; Klein, M. P.; Bender, C. J.; Babcock, G. T. *Biochemistry* **1993**, *32*, 13 718.